NANO LETTERS

Letter

pubs.acs.org/NanoLett

Ultraclean Emission from InAsP Quantum Dots in Defect-Free Wurtzite InP Nanowires

Dan Dalacu,*[,†] Khaled Mnaymneh,[†] Jean Lapointe,[†] Xiaohua Wu,[†] Philip J. Poole,[†] Gabriele Bulgarini,[‡] Val Zwiller,[‡] and Michael E. Reimer[‡]

[†]National Research Council of Canada, Ottawa, Canada, K1A 0R6

[‡]Kavli Institute of Nanoscience, Delft University of Technology, 2600 GA Delft, The Netherlands

Supporting Information

ABSTRACT: We report on the ultraclean emission from single quantum dots embedded in pure wurtzite nanowires. Using a two-step growth process combining selective-area and vapor−liquid−solid epitaxy, we grow defect-free wurtzite InP nanowires with embedded InAsP quantum dots, which are clad to diameters sufficient for waveguiding at $\lambda \sim 950$ nm. The absence of nearby traps, at both the nanowire surface and along its length in the vicinity of the quantum dot, manifests in excitonic transitions of high spectral purity. Narrow emission line widths (30 μeV) and very-pure single photon emission with a probability of multiphoton emission below 1% are achieved, both of which were not possible in previous work where stacking fault densities were significantly higher.

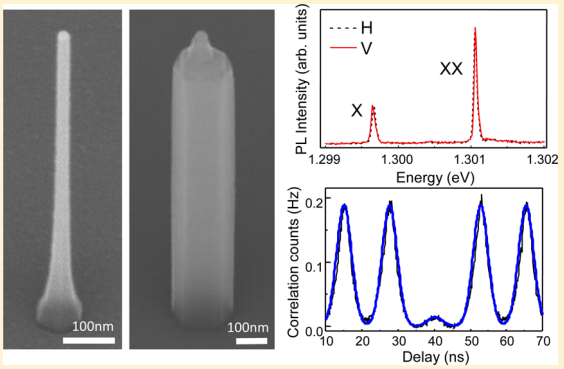

KEYWORDS: *Nanowire, Qauntum dot, InAs/InP, Single photon source, Chemical beam epitaxy, Selective-area VLS growth*

Quantum dots embedded in nanowire waveguides with a controlled shape show great promise as efficient sources of single photons and entangled photon pairs for use in quantum cryptography and quantum computing. Near-unity coupling of an emitted photon to the guided mode of the nanowire is predicted for an ideally polarized emitter that is positioned exactly on the nanowire axis with an appropriate diameter.[1] Single-photon flux collection efficiencies of 72% have been obtained for devices fabricated using standard top-down processing of self-assembled InAs quantum dots.[2] However, in top-down random-based approaches, quantum dots can also be found off the nanowire axis, which therefore dramatically decreases the efficiency of the single-photon source.[3] This random-based approach of fabricating waveguides around multiple quantum dots is overcome by a bottom-up growth approach,[4−7] which ensures that devices contain only a single quantum dot that is ideally located on the axis of the nanowire. The bottom-up growth approach also promises collection efficiencies exceeding 90% by precisely controlling the nanowire shape with an ultra smooth taper toward the tip[7] and integration of a thin dielectric between the nanowire and gold mirror.[8]

Bottom-up nanowires obtained by the vapor−liquid−solid (VLS) growth mechanism are generally polytypic, with alternating sections of zincblende (ZB) and wurtzite (WZ) phases along their lengths.[9] The heterostructure formed between these two crystal phases have a staggered type II band alignment, with holes confined in the WZ phase and electrons in the ZB phase.[10] The presence of these charge traps in close proximity to a quantum dot is detrimental, leading to enhanced spectral diffusion associated with space charge fluctuations.[11] This affects the spectral purity of the excitonic emission and the ability of the source to produce indistinguishable photons, which is important for many quantum information applications, such as linear-optical quantum computation.[12] In addition, spatially indirect transitions from these confined carriers produce unwanted background emission with energies spanning the ZB and WZ bandgaps.[13] It is therefore highly desirable to have only a single crystal phase in photonic nanowire-based single-photon sources to substantially improve the optical quality of the emitter and to reduce the multiple photon emission associated with the background emission due to the presence of the stacking faults (i.e., ZB sections in WZ nanowires or vice versa).

In this work, we demonstrate the impact of a growth method to dramatically reduce the number of stacking faults in the vicinity of the quantum dot and therefore reduce by at least an order of magnitude the emission line width of a single InAsP quantum dot embedded in a pure WZ InP nanowire waveguide. The removal of stacking faults in the nanowire results in a suppression of background emission for our single-photon source, corresponding to multiphoton emission below 1%. We emphasize that the ultraclean quantum dot emission that we

Received: September 6, 2012
Revised: October 10, 2012

   dx.doi.org/10.1021/nl303327h | *Nano Lett.* XXXX, XXX, XXX−XXX

demonstrate was not obtainable in our previous studies on the same material system in the presence of stacking faults.[7,14]

We obtain efficient emitters with a high crystal phase purity by using a two-step growth process, first growing the nanowire core which contains the InAsP dot, and then cladding that core. The crystal structure of the cladding is seeded by the core, which means that it determines the phase purity of the final nanowire waveguide, in this case pure WZ. Using cores of sufficiently small diameters[15] and suitable growth conditions[16] we obtain defect-free WZ nanowires. We emphasize that the size of the nanowire core also determines the final quantum dot diameter. The cladding is required for efficient single-photon emission since it (i) removes the detrimental effects associated with the semiconductor surface (similarly to capping of self-assembled quantum dots) and (ii) increases the coupling of emitted photons to external collection optics.[1,7,17] The crystal phase purity is established by photoluminescence (PL) spectroscopy and transmission electron microscopy (TEM) analysis.

The growth process (see Methods) combines selective-area (SA) and VLS epitaxy as outlined in Figure 1. Growth was

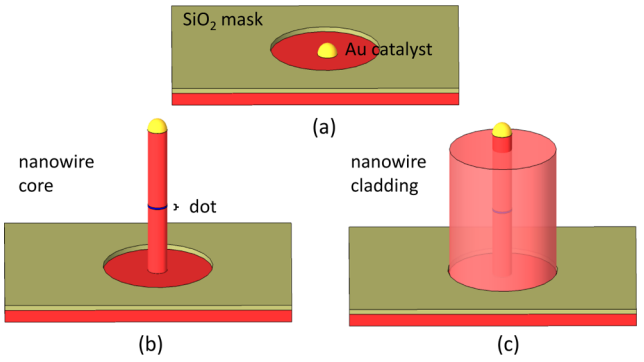

Figure 1. Schematic illustration of the SA-VLS growth process: (a) The nanowires are grown on a patterned substrate consisting of circular openings in a SiO_2 mask in which gold catalysts are deposited by a self-aligned lift-off process. (b) The nanowire core is grown using growth conditions that promote catalyzed growth while minimizing substrate growth. (c) Conversely, the nanowire cladding is grown by minimizing catalyzed growth while promoting substrate growth.

carried out on substrates consisting of 20 nm gold particles centered in circular openings in a SiO_2 mask on an InP wafer, as shown in Figure 1a. In the first step of the process, growth conditions were used that promote VLS growth of the nanowire core (Figure 1b). At this stage, the quantum dot was also grown in the nanowire core, approximately 200 nm from the substrate surface. In the second step of the process the growth conditions were changed resulting in a cladding of the nanowire, the dimensions of which are dictated by the annulus of exposed InP at the base of the nanowire, as shown in Figure 1c. We emphasize that the cladding growth mode is only possible because of the selective nature of the patterned-substrate epitaxy. Without the selectivity provided by the SiO_2 mask, substrate growth would compete with growth at the nanowire base and severely limit the ability to clad.[18]

The final result of the two-step growth process is shown in Figure 2. After the first step an array of nanowire cores is obtained (Figure 2a). Typical nanowire dimensions are 20 nm in diameter and 750 nm in height. A single nanowire core is shown in Figure 2b, which has a tapered pedestal at the base as the VLS growth conditions used do not completely suppress

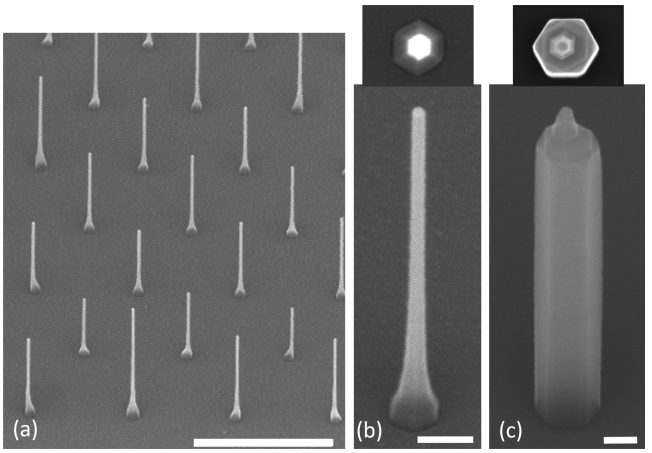

Figure 2. SEM images of nanowires. The three main images are viewed at 45°, while the upper panels in b and c are viewed at normal incidence. (a) Array of nanowire cores. Scale bar indicates 1 μm. (b) A single nanowire core grown with a 20 nm gold catalyst. The upper panel highlights the hexagonal base. (c) Clad nanowire. Scale bar in b and c is 100 nm.

substrate growth. Figure 2c shows a clad nanowire. The growth of the cladding proceeds up the nanowire core from the base, eventually cladding the entire core. Continued growth after this point occurs laterally, with the nanowire overgrowing the 100 nm diameter patterned hole to reach a final diameter of 250 nm. This nanowire diameter allows for very efficient coupling of light emitted from the nanowire into the collection optics.[7,17] We note that the growth conditions used during radial growth to form the cladding do not completely quench VLS growth, resulting in clad nanowires nearly twice as tall as the nanowire cores.

The upper panel in Figure 3 shows the PL spectrum of a single InP nanowire without a quantum dot. It comprises of a single peak centered at 1.49 eV consistent with band to band electron–hole recombination in wurtzite InP[19] and has been previously observed.[20−23] There is no evidence of emission related to crystal imperfections, typically observed in the energy range spanning from 1.35 to 1.49 eV.[13,24] The clean PL is consistent with TEM analysis of the nanowire core (see Supporting Information), which revealed an extremely low stacking fault density of less than one per micrometer. Due to the very high crystal phase purity of the InP nanowire, the line width of the WZ peak at low excitation powers (30 mW/cm^2) is relatively narrow (3.7 meV), as compared to previous measurements on single nanowires (5–20 meV).[21−23]

The lower panel of Figure 3 shows the power-dependent PL from a single nanowire containing a single InAsP quantum dot. The low excitation spectrum consists of a single peak around 1.3 eV corresponding to emission from transitions in the *s*-shell. Note that, at low excitation, the WZ emission is absent, indicating very efficient carrier capture by the quantum dot. With increasing excitation intensity, higher level shells in the quantum dot are progressively populated, with confined *p*- and *d*-orbitals at energies of 20 and 45 meV, respectively, above the *s*-shell. The weak feature at 1.44 eV present in all of the spectra in Figure 3 is observed in all our samples and is associated with emission from donor–acceptor levels in the nanowire.[22]

Figure 4a shows a high resolution PL spectrum of a typical dot excited with 50 nW power, which saturates the ground-state transition. The three dominant peaks in the *s*-shell around 1.3

dx.doi.org/10.1021/nl303327h | *Nano Lett.* XXXX, XXX, XXX–XXX

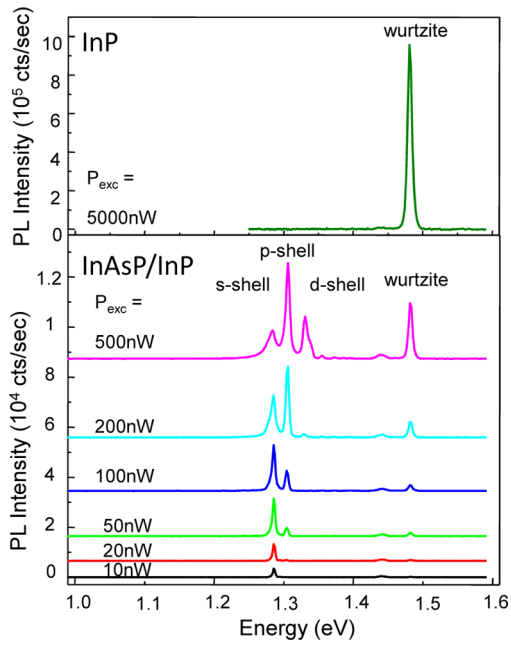

Figure 3. Upper panel: PL from a single WZ nanowire showing a single peak corresponding to band-to-band electron−hole recombination in WZ InP. Lower panel: power dependent PL of a WZ nanowire containing a single InAsP quantum dot. In addition to the WZ peak, three confined orbitals are observed upon increasing the excitation power.

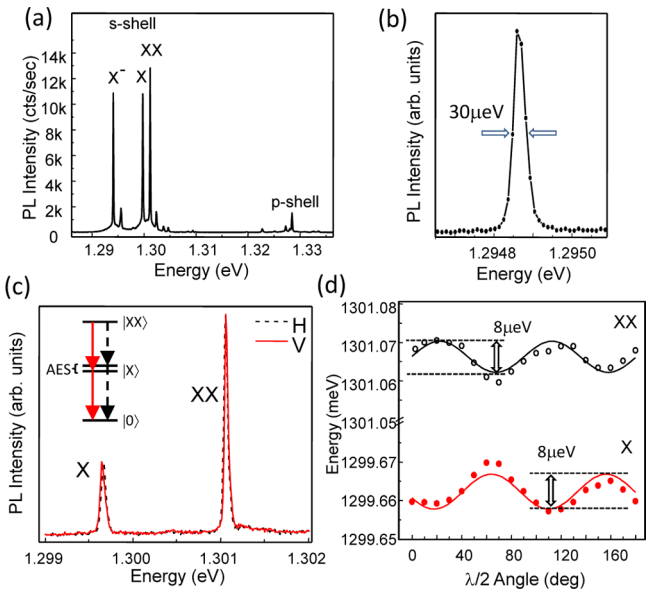

Figure 4. (a) PL spectrum of a typical quantum dot pumped at saturation. (b) Low excitation spectrum of a charged exciton showing the narrow emission line width. (c) Polarized PL spectra of the X and XX transitions where H (V) indicates horizontally (vertically) polarized emission. Inset: schematic of biexciton−exciton radiative cascade in the presence of an anisotropic exchange splitting. (d) Peak energies extracted from Lorentzian fits of the polarized X and XX emission as a function of half-wave plate angle.

eV are identified as the exciton (X), biexciton (XX), and charged exciton (X^-) from power-dependent PL measurements (see Supporting Information) and polarization-sensitive PL measurements, discussed below. The assignment of the X^- peak comes from comparison with data from ref 25 where electrical gating allowed an unambiguous determination of the charge state. Typical measured emission line widths are 30 μeV (resolution-limit of the spectrometer), as shown in Figure 4b for a X^- transition at ∼1.295 eV. Line width broadening in quantum dots can occur, in large part, due to a fluctuating charge environment around the dot. The trapping and untrapping of charges close to the dot changes its electrostatic environment, resulting in a fluctuating Stark shift of the emission energy. Stacking faults act as very efficient charge traps, trapping the charge along the axis of the wire but allowing it to move perpendicular to the wire axis. It is therefore expected that the presence of stacking faults in close proximity to a dot results in significant broadening of the emission lines. Such broadening was observed in our previous quantum dots grown in nanowires with a higher stacking fault density,[7,14] where the measured line widths were typically ∼400−700 μeV. The narrow emission line widths measured here suggests that this broadening mechanism is strongly suppressed in these nanowires. This is consistent with results in other laboratories[6,26] where line widths of similar samples range from ∼100 μeV to several meV with quoted stacking fault densities as high as 1 per 10 nm.[26]

Unlike self-assembled quantum dots grown on (001) substrates, [111]-oriented nanowire quantum dots on (111)B substrates are predicted to have a vanishingly small anisotropic exchange splitting, which is important for generation of entangled photon pairs.[27] The narrow emission line width that we observe allows for analysis of the fine structure splitting arising from the electron and hole exchange interaction.[28] Analysis of the fine structure splitting is shown in Figure 4c and d, which is obtained by rotating a half-wave plate in front of a fixed Glan−Thomson polarizer[29,30] at the entrance of the spectrometer. The polarized doublet of X and XX is shown in Figure 4c, with the XX peak ∼1.5 meV above the X peak. The polarized PL emission of the X and XX transitions exhibit a slight blue (red) shift of the horizontally polarized X (XX) peak compared to the vertically polarized X (XX) peak, as expected from the biexciton exciton radiative cascade.[31] Figure 4d shows shows the peak energy of X and XX obtained from Lorentzian fits plotted against half-wave plate angle. The amplitude of a sine curve fit to the data in Figure 4d yields a very small splitting of 8 μeV, although not as small as predicted in ref 27. Polarization-resolved emission from the third peak typically observed in the *s*-shell shows no exchange splitting, consistent with emission from a singly charged exciton.[28,30] This behavior is typical of the eight nanowires on which we measured high resolution polarization-resolved PL.

Finally, we demonstrate suppressed multiphoton emission of our single-photon source in Figure 5, which would generally be increased in bottom-up grown nanowires as a result of background emission arising from the presence of stacking faults in the nanowire. We perform second-order correlation measurements of the exciton line at saturation for two samples with different nanowire diameters. Remarkably, in Figure 5a we observe the absence of coincidence counts at zero time delay, which is an indication of very pure single-photon emission. The nonzero background correlation counts are due to the long exciton lifetime of the quantum dot as it is re-excited before the emission has decayed to zero. From a fit to the data by theory (solid blue line), we can conclude that multiphoton emission is suppressed below 1%, which is similar to state-of-the-art self-assembled quantum dots in photonic nanowires.[2] We note that the very low $g^2(0)$ that we observe here for bottom-up grown

dx.doi.org/10.1021/nl303327h | *Nano Lett.* XXXX, XXX, XXX−XXX

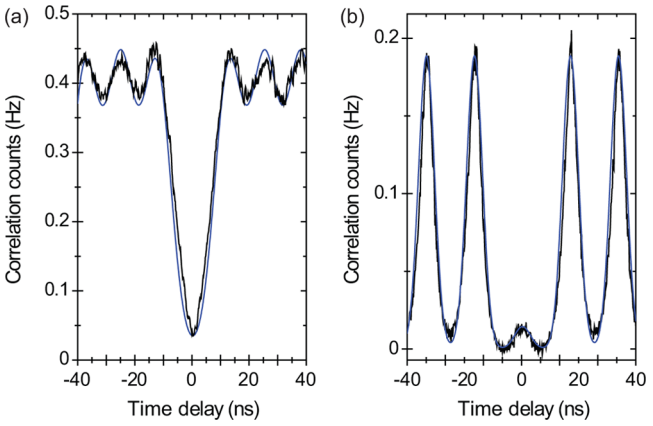

Figure 5. Second-order correlation trace of exciton line (black) at saturation for two different nanowire diameters. From a fit to the data by theory (blue), we obtain $g^2(0) < 0.005$ in a and $g^2(0) = 0.08$ in b with corresponding exciton lifetimes of 8.9 ns and 2 ns, respectively. Identical lifetimes were also measured directly.

nanowires is only possible when the background emission is absent as a result of stacking fault free nanowires. The long exciton lifetime (8.9 ns) obtained in Figure 5a is expected and observed in previous work when the fundamental guided mode is not optimally confined in the nanowire.[3,17] In such circumstances, the spontaneous emission decay rate of the quantum dot into the fundamental guided mode is comparable to the emission decay rate into nonguided leaky modes in vacuum.[3,17] As the nanowire diameter is increased, the fundamental guided mode becomes more tightly confined in the nanowire, and the quantum dot emits photons with an increased rate, approaching the decay rate for the same emitter in bulk InP.[17] The increased decay rate and thus shortening of the exciton lifetime (2 ns) can be observed in Figure 5b. We note here that the $g^2(0)$ is slightly increased as compared to Figure 5a since there are other nanowire quantum dots within the laser excitation spot.

In summary, we have demonstrated a growth method to control the stacking fault density in nanowire waveguides containing a single InAsP quantum dot on its axis in a reproducible manner. The crystal phase purity of the nanowire combined with the thick cladding mitigates the effects of spectral diffusion associated with nearby trapped charges. In consequence, spectrally pure transitions with resolution-limited optical line widths of 30 μeV are obtained that are at least 1 order of magnitude smaller than previous works in the presence of stacking faults. Contrary to predictions made for InAsP quantum dots in [111]-oriented InP nanowires, we measure a nonvanishing anisotropic exchange splitting of the exciton transition equal to 8 μeV. Finally, due to the absence of background emission owing to the presence of stacking faults, we measure very pure single-photon emission with a probability of multiphoton emission below 1%. This very pure single-photon emission combined with the high count rates and narrow optical line widths reveals the potential of quantum dots in bottom-up grown nanowires for future quantum technologies.

Methods. *Nanowire Growth.* The InAsP/InP nanowire quantum dots were grown using chemical beam epitaxy (CBE) with trimethylindium (TMI) and precracked PH_3 and AsH_3 sources. The nanowires were grown on a SiO_2-patterned (111) B InP substrate consisting of circular holes opened up in the oxide mask using electron-beam lithography and a hydrofluoric acid wet-etch. Au was deposited in these holes using a self-aligned lift-off process, which allows the nanowires to be positioned at known locations on the substrate.[18] The thickness of the deposited gold is chosen to give 20 nm diameter particles.

The nanowire core is grown under conditions which promote VLS growth of pure WZ nanowires for gold particles 20 nm in diameter. To promote catalyzed growth and suppress substrate growth entails growing at low temperature, in particular, we use 420 °C. The dot was incorporated by switching from a PH_3 to an AsH_3 overpressure for 3 s after 15 min of growth, which places the dot approximately 200 nm from the substrate surface. The overall growth time of the nanowire core was 26 min. We obtain defect-free WZ nanowires for TMI fluxes below a certain threshold value, and this value is dependent on the group V flux.[16] In SA-VLS, the growth rate depends on the Au catalyst size and is nonlinear, increasing with increasing nanowire height.[18] For the nanowires studied here the TMI flux used for defect-free cores was equivalent to that used for a planar InP growth rate of 0.1 μm/h on (001) InP substrates at a temperature of 500 °C. The PH_3 flow was 3 sccm.

To clad the nanowire core we used conditions that promoted substrate growth while suppressing VLS growth at the nanowire tip. Previously, we have used temperature to adjust the relative incorporation rates with higher temperature activating substrate growth while quenching catalyzed growth.[14] We have also found that increasing the group V flux results in a similar change in relative incorporation rates, and in this study, the growth mode is switched by increasing the PH_3 flow from 3 to 9 sccm. The growth time for the cladding was 94 min. Although VLS growth is not completely quenched (the clad nanowires are nearly twice as tall as the nanowire cores), it is significantly suppressed considering growth times of 26 and 94 min for the core and cladding, respectively. Without increasing the PH_3 by a factor of 3 the nanowire would by expected to be greater than 12 μm tall after the additional 94 min of growth, rather than the 1.5 μm observed.

Optical Spectroscopy. Optical measurements on individual nanowires were performed with the wires still attached to the (111)B InP substrate. The measurements were done at 4.2 K in a continuous flow helium cryostat using nonresonant, above bandgap excitation through a 50× microscope objective (N.A. = 0.65) with a ~2 μm spot size. The PL was collected through the same microscope objective, dispersed using a grating spectrometer. Low resolution spectra were taken with a 0.257 m spectrometer and detected using a liquid-nitrogen cooled InGaAs diode array, and high-resolution spectra were measured with a 0.64 m spectrometer and detected using a liquid-nitrogen cooled silicon CCD. The second-order correlation measurements were performed in a standard Hanbury–Brown and Twiss setup. The quantum dot was excited above bandgap with a Ti:sapphire laser at 744 nm using 3 ps laser pulses at a repetition rate of 76 MHz, and the emitted photons were detected by Si avalanche photodiodes.

■ ASSOCIATED CONTENT

Supporting Information

Additional TEM analysis and PL measurements. This material is available free of charge via the Internet at http://pubs.acs.org.

dx.doi.org/10.1021/nl303327h | *Nano Lett.* XXXX, XXX, XXX–XXX

AUTHOR INFORMATION

Corresponding Author

*E-mail: dan.dalacu@nrc-cnrc.gc.ca.

Notes

The authors declare no competing financial interest.

REFERENCES

(1) Friedler, I.; Sauvan, C.; Hugonin, J. P.; Lalanne, P.; Claudon, J.; Gérard, J. M. *Opt. Express* **2009**, *17*, 2095.

(2) Claudon, J.; Bleuse, J.; Malik, N. S.; Bazin, M.; Jaffrennou, P.; Gregersen, N.; Sauvan, C.; Lalanne, P.; Gérard, J.-M. *Nat. Photon.* **2010**, *4*, 174.

(3) Bleuse, J.; Claudon, J.; Creasey, M.; Gérard, N. S. M. J.-M.; Maksymov, I.; Hugonin, J.-P.; Lalanne, P. *Phys. Rev. Lett.* **2011**, *106*, 103601.

(4) Borgström, M.; Zwiller, V.; Müller, E.; Imamoglu, A. *Nano Lett.* **2005**, *5*, 1439−1443.

(5) Tribu, A.; Sallen, G.; Aichele, T.; André, R.; Poizat, J.-P.; Bougerol, C.; Tatarenko, S.; Kheng, K. *Nano Lett.* **2008**, *8*, 4326−4329.

(6) Heinrich, J.; Hugenberger, A.; Heindel, T.; Reitzenstein, S.; Höfling, S.; Worschech, L.; Forchel, A. *Appl. Phys. Lett.* **2010**, *96*, 211117.

(7) Reimer, M. E.; Bulgarini, G.; Akopian, N.; Hocevar, M.; Bavinck, M. B.; Verheijen, M. A.; Bakkers, E. P. A. M.; Kouwenhoven, L. P.; Zwiller, V. *Nat. Commun.* **2012**, *3*, 737.

(8) Friedler, I.; Lalanne, P.; Hugonin, J. P.; Claudon, J.; Gérard, J. M.; Beveratos, A.; Robert-Philip, I. *Opt. Lett.* **2008**, *33*, 2635−2637.

(9) Caroff, P.; Bolinsson, J.; Johansson, J. *IEEE J. Sel. Top. Quant. Elect.* **2011**, *17*, 829.

(10) Bao, J.; Bell, D. C.; Capasso, F.; Wagner, J. B.; Mårtensson, T.; Trägårdh, J.; Samuelson, L. *Nano Lett.* **2008**, *8*, 836−841.

(11) Sallen, G.; Tribu, A.; Aichele, T.; André, R.; Besombes, L.; Bougerol, S.; Richard, M.; Tatarenko, S.; Kheng, K.; Poizat, J.-P. *Phys. Rev. B* **2011**, *84*, 041405.

(12) Knill, E.; Laflamme, R.; Milburn, G. *Nature* **2001**, *409*, 46−52.

(13) Akopian, N.; Patriarche, G.; Liu, L.; Harmand, J.-C.; Zwiller, V. *Nano Lett.* **2010**, *10*, 1198−1201.

(14) Dalacu, D.; Mnaymneh, K.; Wu, X.; Lapointe, J.; Aers, G. C.; Poole, P. J.; Williams, R. L. *Appl. Phys. Lett.* **2011**, *98*, 251101.

(15) Johansson, J.; Dick, K. A.; Caroff, P.; Messing, M. E.; Bolinsson, J.; Deppert, K.; Samuelson, L *J. Phys. Chem. C* **2010**, *114*, 3837−3842.

(16) Poole, P. J.; Dalacu, D.; Wu, X.; Lapointe, J.; Mnaymneh, K. *Nanotechnology* **2012**, *23*, 385205.

(17) Bulgarini, G.; Reimer, M. E.; Hocevar, T. Z. M.; Bakkers, E. P. A. M.; Kouwenhoven, L. P.; Zwiller, V. *Appl. Phys. Lett.* **2012**, *100*, 121106.

(18) Dalacu, D.; Kam, A.; Austing, D. G.; Wu, X.; Lapointe, J.; Aers, G. C.; Poole, P. J. *Nanotechnology* **2009**, *20*, 395602.

(19) Dacal, L. C. O.; Cantarero, A. *Solid State Commun.* **2011**, *151*, 781−784.

(20) Mohan, P.; Motohisa, J.; Fukui, T. *Nanotechnology* **2005**, *16*, 2903−2970.

(21) Mishra, A.; Titova, L. V.; Hoang, T. B.; Smith, L. M.; Yarrison-Rice, J. M.; Joyce, H. J.; Gao, Q.; Tan, H. H.; Jagadish, C. *Appl. Phys. Lett.* **2007**, *91*, 263104.

(22) Gadret, E. G.; Dias, G. O.; Dacal, L. C. O.; de Lima, J. M. M.; Ruffo, C. V. R. S.; Iikawa, F.; Brasil, M. J. S. P.; Chiaramonte, T.; Cotta, M. A.; Tizei, L. H. G.; Ugarte, D.; Cantarero, A. *Phys. Rev. B* **2010**, *182*, 125327.

(23) Chauvin, N.; Alouane, M. H. H.; Anufriev, R.; Khmissi, H.; Naji, K.; Patriarche, G.; Bru-Chevallier, C.; Gendry, M. *Appl. Phys. Lett.* **2012**, *100*, 011906.

(24) Jancu, J.-M.; Gauthron, K.; Largeau, L.; Patriarche, G.; Harmand, J.-C.; Voison, P. *Appl. Phys. Lett.* **2010**, *97*, 041910.

(25) Reimer, M. E.; van Kouwen, M. P.; Hidma, A. W.; van Weert, M. H. M.; Bakkers, E. P. A. M.; Kouwenhoven, L. P.; Zwiller, V. *Nano Lett.* **2010**, *11*, 645−650.

(26) Sköld, N.; Pistol, M.-K.; Dick, K. A.; Pryor, C.; Wagner, J. B.; Karlsson, L. S.; Samuelson, L. *Phys. Rev. B* **2009**, *80*, 041312(R).

(27) Singh, R.; Bester, G. *Phys. Rev. Lett.* **2009**, *103*, 063601.

(28) Bayer, M.; Ortner, G.; Stern, O.; Kuther, A.; Gorbunov, A. A.; Forchel, A.; Hawrylak, P.; Fafard, S.; Hinzer, K.; Reinecke, T. L.; Walck, S. N.; Reithmaier, J. P.; Klopf, F.; Schäfer, F. *Phys. Rev. B* **2002**, *65*, 195315.

(29) Kowalik, K.; Krebs, O.; Lemlâitre, S. L. A.; Senellart, P.; Voisin, P.; Gaj, J. A. *Appl. Phys. Lett.* **2005**, *86*, 041907.

(30) Reimer, M. E.; Dalacu, D.; Lapointe, J.; Poole, P. J.; Kim, D.; Aers, G. C.; McKinnon, W. R.; Williams, R. L. *Appl. Phys. Lett.* **2009**, *94*, 011108.

(31) Young, R. J.; Stevenson, R. M.; Shields, A. J.; Atkinson, P.; Cooper, K.; Ritchie, D. A.; Groom, K. M.; Tartakovskii, A. I.; Skolnick, M. S. *Phys. Rev. B* **2005**, *72*, 113305.